ACS APPLIED MATERIALS & INTERFACES

Letter

www.acsami.org

Printable Highly Catalytic Pt- and TCO-Free Counter Electrode for Dye-Sensitized Solar Cells

Jian He, Lawrence Tien Lin Lee, Shihang Yang, Quan Li, Xudong Xiao, and Tao Chen*

Department of Physics, the Chinese University of Hong Kong, Shatin, Hong Kong SAR, China

Supporting Information

ABSTRACT: Here we show that a counter electrode based on carbon network supported Cu_2ZnSnS_4 nanodots on Mo-coated soda-lime glass for dye-sensitized solar cells can outperform the conventional best electrode with Pt nanoparticles on the fluorine-doped SnO_2 conducting glass. In the as-developed electrode, all of the elements are of high abundance ratios with low materials cost. The fabrication is scalable because it is conducted by a screen-printing based approach. Therefore, this research lays a solid ground for the large area fabrication of high-performance dye-sensitized solar cell at reduced material cost.

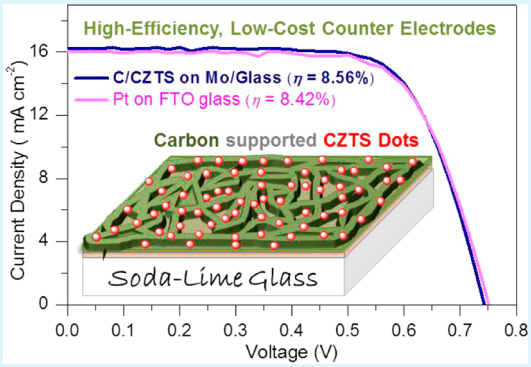

KEYWORDS: *Cu_2ZnSnS_4, nanostructure, carbon, catalyst, solar cell, counter electrode*

Dye-sensitized solar cells (DSSCs) have received renewed interest because of their low fabrication cost, environmental friendliness, and reasonably high power conversion efficiency (PCE, η).[1−3] Typically, the device consists of dye-adsorbed TiO_2 nanoparticle network, filled with electrolyte containing redox couples such as I^-/I_3^-, and counter electrode (CE). Conventionally, Pt nanoparticle, as catalyst, on the F:SnO_2 (FTO) glass, is applied as the CE, which shows highly efficient catalytic characteristics.[3−5] However, as a noble metal, Pt features high cost and low abundance ratio in nature. To reduce the materials cost, much efforts have been put into the development of low-cost catalyst and a variety of materials based on carbon, metal carbide, nitride, and chalcognide have been examined and shown promising catalytic performance.[6−13] It is noted that all of the investigations are based on the FTO coated glass. In fact, the FTO glass accounts for nearly 60% of the total cost in DSSCs.[14] Therefore, to explore low cost alternatives to FTO glass is of practical significance. Nevertheless, the exploration of high-efficiency cost-effective conducting substrate is less successful when compared with the development of Pt-free catalyst. To date, conducting polymers such as PEDOT,[14] carbon fiber,[15] PEDOT:PSS,[16] and metal nanowire network[17] have been examined for the conducting substrates. However, all of them show much poorer performance than the FTO-based substrates, mainly due to the large sheet resistance. Herein, we demonstrate that Mo-coated soda-lime glass (Mo/glass), coupling with carbon supported Cu_2ZnSnS_4 (CZTS) nanodots, can outperform FTO when used as conducting glass for the CE of DSSCs. The use of Mo/glass is also under the consideration that its work function (4.6 eV) is quite close to the FTO (4.4 eV). This research demonstrates that a Pt- and TCO-free CE can outperform the "champion" CE based on Pt/FTO.

Considering that the ultimate goal of DSSC investigation is for practical large-area applications, we aim at developing screen printable fabrication procedure. In order to reduce the materials cost as much as possible, we intentionally adopt easily attainable and low-cost chemical compounds $CuCl_2{\cdot}2H_2O$, $ZnCl_2$ and $SnCl_4{\cdot}5H_2O$ as the CZTS precursors, ethylcellucose as binder, and *t*-butanol and ethanol as solvents to tune the viscosity of the paste. The details for the paste preparation are provided in the Supporting Information. The paste coating is compatible with the conventional printing techniques. Afterwards, heating the substrate at 550 °C in H_2S/Ar mixture gas at 50−100 Pa for 60−80 min can generate carbon-supported CZTS nanodots (Figure 1a). To make a systematic investigation, we also conducted the synthesis in selenium vapor to obtain carbon-supported $Cu_2ZnSnSe_4$ (CZTSe) nanodots.

To determine the phase purity of the as-synthesized materials, we first performed X-ray diffraction (XRD) characterization. For the sample annealed in H_2S/Ar gas, the major XRD diffraction peaks appears at 28.2, 47.1, and 55.9° (Figure 1b), which can be indexed as (112), (220), and (312) planes of CZTS (JCPDS Card No. 26-0575). Additionally, the lattice parameter of the CZTS is calculated to a = 0.5427 nm and c = 1.0848 nm, consistent with the reported results.[18] However, the phase purity of CZTS cannot be identified by XRD alone

Received: December 13, 2013
Accepted: January 27, 2014
Published: January 27, 2014

   dx.doi.org/10.1021/am4057375 | *ACS Appl. Mater. Interfaces* 2014, 6, 2224−2229

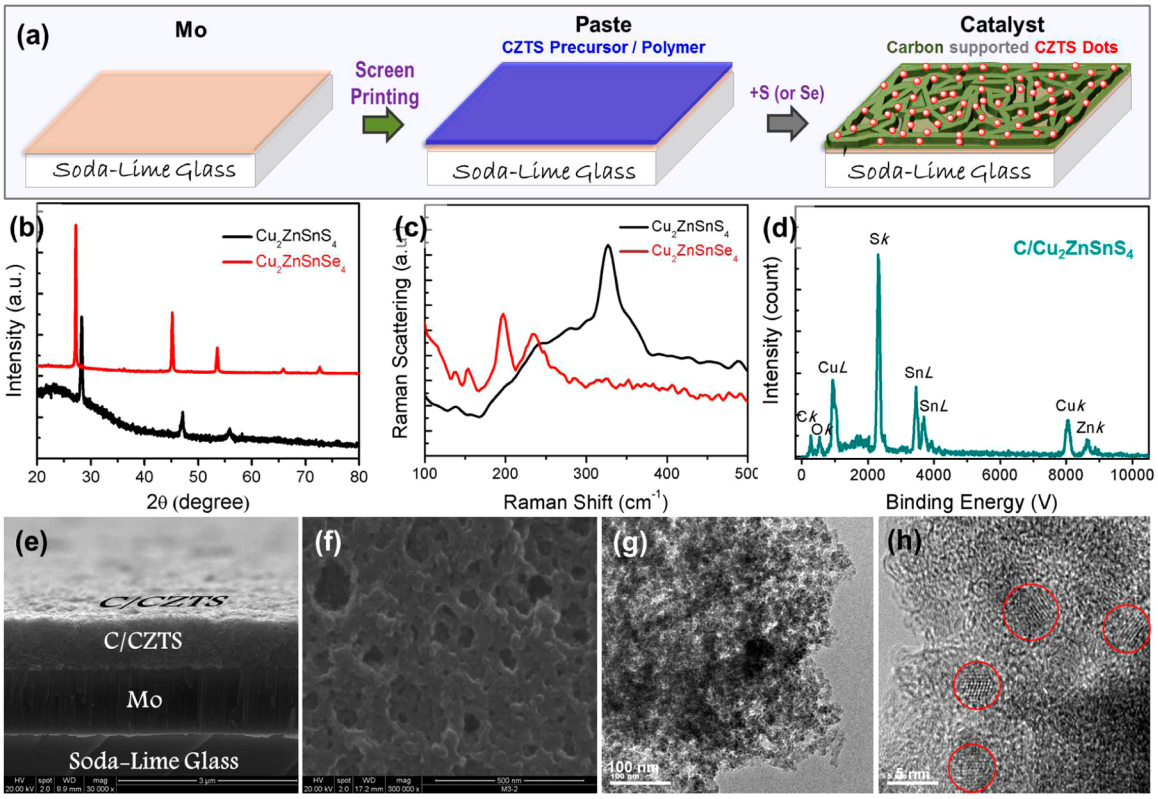

Figure 1. (a) Schematic illustration of the methodology for the fabrication of carbon-supported CZTS nanodots on Mo-coated soda-lime glass, where the precursor for the paste are $CuCl_2{\cdot}2H_2O$, $SnCl_4{\cdot}5H_2O$, $ZnCl_2$, ethyl cellulose, *t*-terpinol, and ethanol; (b) XRD patterns of the as-prepared catalyst; (c) Raman spectra of the as-synthesized catalyst on Mo-coated glass; (d) EDS of the carbon-supported CZTS nanodots; (e, f) SEM images of the cross-section of the as-synthesized catalyst on Mo-coated glass and the surface morphology; (g, h) HRTEM images of the as-synthesized carbon-supported CZTS nanodots, the CZTS nanodots are marked with circles in f.

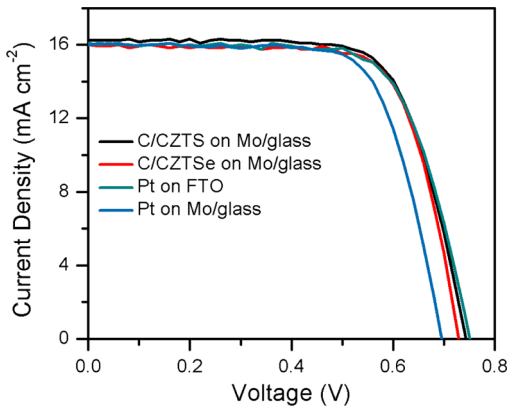

Figure 2. Photocurrent density–voltage characteristics of the devices with C/CZTS and C/CZTSe on Mo/glass, Pt/FTO glass, and Pt/Mo glass as counter electrodes.

Table 1. Photovoltaic Parameters of the Dye-Sensitized Solar Cells with Different Counter Electrodes: Carbon-Supported Cu_2ZnSnS_4 Nanodots and Carbon-Supported $Cu_2ZnSnSe_4$ Nanodots on Mo-Coated Soda-Lime Glass, and Pt Nanoparticles on FTO and Mo/Glass Surface, Measured under 1 Sun Illumination (AM 1.5 G, 100 mW cm^{-2})

counter electrode	PCE (%)	J_{sc} (mA cm^{-2})	V_{oc} (V)	FF (%)
$C/Cu_2ZnSnS_4/Mo$[a]	8.56	16.2	0.74	71.0
$C/Cu_2ZnSnSe_4/Mo$	8.45	16.1	0.73	71.8
Pt/FTO[b]	8.42	14.8	0.75	73.0
Pt/Mo	7.92	15.99	0.70	71.3

[a]Carbon-supported Cu_2ZnSnS_4 on Mo-coated soda-lime glass as the counter electrode. [b]Traditional Pt nanoparticles on FTO surface as counter electrode.

because ZnS and Cu_2SnS_3 exhibit similar patterns. In this case, Raman scattering characterization was additionally employed to identify the materials. The result shows Raman shift at 327 cm^{-1} (Figure 1c), which is the typical Raman scattering of CZTS.[19] Since the annealing is conducted in reducing gas (H_2S/Ar), the carbonization of the polymer precursor should occur. Therefore, energy-dispersive X-ray spectroscopy (EDS) was obtained to examine the composition. It is found that carbon atoms account for an atomic percentage of 40% in the film (Figure 1d). In the selenized product, the XRD shows typical CZTSe pattern, with 2θ appears at 27.2, 45.2, 53.6, 65.9, and 72.6° (Figure 1b), corresponding to the (112), (204), (312), (008), and (316) crystal planes of CZTSe. The Raman scattering shows typical peaks at 197 and 234 cm^{-1} (Figure 1c).[20]

The film thickness and surface morphology were characterized by scanning electron microscopy (SEM). Figure 1e shows the cross-section of the composite carbon and CZTS film on Mo/glass, the average thickness is measured to be 730 nm. The surface of the film presents nanoscale network morphology (Figure 1f). Detailed inspection on the as-synthesized product was performed by high-resolution transmission electron microscopy (HRTEM). It is observed that the CZTS nanodots distribute onto the carbon network (Figure 1g), forming carbon-supported CZTS nanodots; the average

dx.doi.org/10.1021/am4057375 | ACS Appl. Mater. Interfaces 2014, 6, 2224–2229

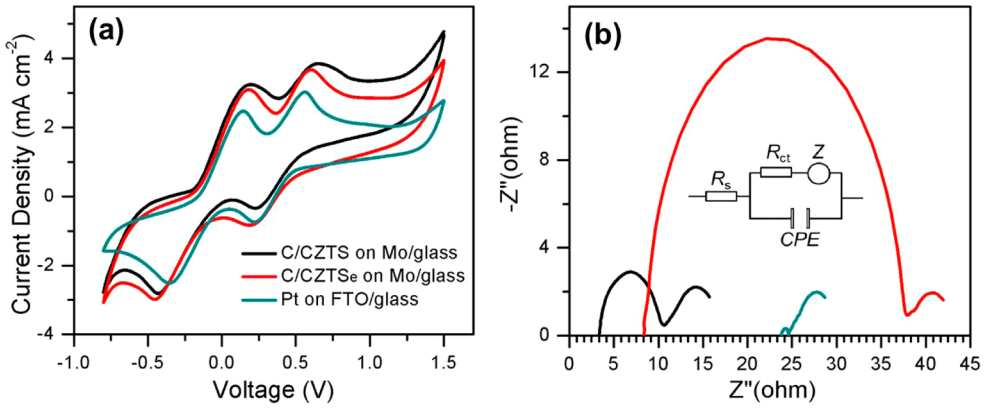

Figure 3. (a) Cyclic voltammetry curves of the devices with C/CZTS and C/CZTSe on Mo/glass and Pt/FTO as working electrodes in a three-electrode system; (b) electrochemical impedance spectra of the symmetric cells based on the electrode with C/CZTS and C/CZTSe on Mo/glass and Pt/FTO.

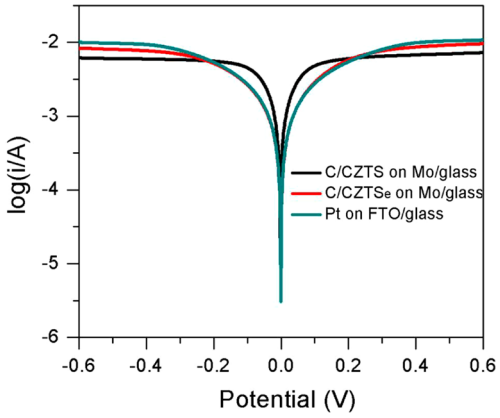

Figure 4. Tafel plots of the symmetric cells based on the electrode with C/CZTS and C/CZTSe on Mo/glass and Pt/FTO.

size of the CZTS nanodots is 3 nm (Figure 1h). The lattice fringe is calculated to be ~0.31 nm, which corresponds to (112) plan of CZTS. The carbon-supported CZTSe network shows similar morphology (see Figure S1 in the Supporting Information) and thickness is ~450 nm.

In the synthesis, the volume change as a result of carbonization and evaporation of terpinol and ethanol during sulfurization or selenization at high temperature contributes to the formation of network, in which the carbonization is the main reason because the reaction carried out in absence of reducing gas (i.e. low degree of carbonization) cannot lead to the nanoscale network (see Figure S2 in the Supporting Information). We also tried to produce CZTS nanodots in absence of polymer binder. However, it is difficult to synthesize well-distributed nanodots on the Mo/glass comparable to that in the C/CZTS film (see Figure S3 in the Supporting Information). Therefore, the use of polymer binder with inorganic salt precursors is critical for the formation of well-defined carbon-network-supported nanodots.

To compare the CE behavior in DSSC, we prepared the device using identical photoanodes that are composed of a 12 μm transparent layer and a 6 μm scattering layer according to our reported method,[21−25] N719 was utilized as the dye sensitizer for all the devices. For each CE, we fabricated three to five devices to obtain reliable results. Figure 2 compares the photovoltaic behavior of the DSSCs with different CEs; the device parameters are tabulated in Table 1 for easy comparison. The DSSC using Pt/FTO as the counter electrode generates a PCE of 8.42%, with short-circuit current density (J_{sc}) of 14.8

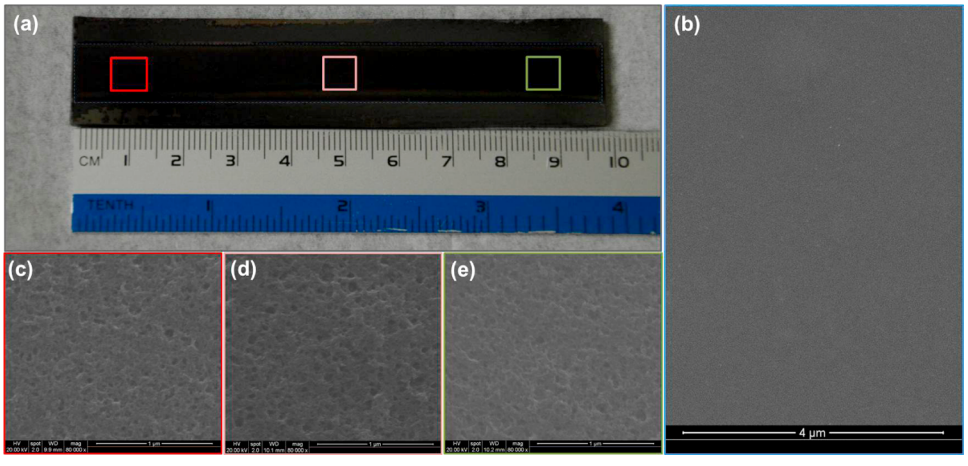

Figure 5. (a) Digital photo of the counter electrode composed of C/CZTSe on Mo/glass with area of 100 mm × 10 mm; (b) low-magnification SEM image of the electrode surface; (c−e) high-magnification SEM images of the C/CZTSe catalyst on the Mo-coated glass from different areas as indicated in a.

dx.doi.org/10.1021/am4057375 | ACS Appl. Mater. Interfaces 2014, 6, 2224−2229

mA cm^{-2}, open-circuit voltage (V_{oc}) of 0.75 V and fill factor (*FF*) of 73.0%. Remarkably, the device with C/CZTS on Mo/glass as CE presents a PCE of 8.56%, with J_{sc} of 16.2 mA cm^{-2}, V_{oc} of 0.74 V, and FF of 71.0%; and the DSSC with C/CZTSe on Mo/glass as CE exhibits a PCE of 8.45% (Figure 2 and Table 1). Both the C/CZTS and C/CZTSe on Mo/glass show better performance that of Pt/FTO, indicating the potential to replace the high-cost Pt nanoparticle on FTO for high-efficiency DSSC.

To further explore the roles played by CZTS in the catalysis, we performed the synthesis in the absence of CZTS precursors. Consequently, the final carbon materials display nonuniform morphology on the Mo substrates (see Figure S4 in the Supporting Information). The DSSC based on this CE presents PCE of 6.01% (see Figure S4 in the Supporting Information), substantially lower those CEs based on carbon supported nanodots or Pt. Actually, in the literature, carbon materials usually display poorer catalytic performance than Pt nanoparticles for CE in DSSC.[26−29] Therefore, the formation of C/CZTS composite catalyst is significant for the high catalytic performance. On the other hand, the CZTS is a narrow band gap semiconducting material;[30,31] it can probably serve as active materials for the light absorption and thus photovoltaic energy conversion. In this regards, we conducted the device fabrication in absence of dye-adsorbed TiO_2 film, the device did not show photovoltaic energy conversion (see Figure S5 in the Supporting Information), indicating that the C/CZTS cannot act as light absorbing materials but only catalyst for the I_3^- reduction reaction.

Because the photoanodes of the devices are identical, the better photovoltaic performance in the Pt- and FTO-free device should be resulted from the excellent catalytic properties. We thus performed comparative study to probe the catalytic mechanism. First, cyclic voltammetry (CV) characterization using a three-electrode system under a I^-/I_3^- system was conducted. The CV curves of I^-/I_3^- redox reaction on the counter electrodes present similar shape (Figure 3a), where two pairs of redox peaks appear in each of the system. The left pair of peaks is corresponding to the reduction (reaction 1), whereas the right pair represents the oxidation of I_2 (reaction 2).

$$I_3^- + 2e^- \rightleftarrows 3I^- \quad (1)$$

$$3I_2 + 2e^- \rightleftarrows 2I_3^- \quad (2)$$

Reaction 1 is pertinent to the DSSC performance, thus we pay special attention into this reaction. The peak positions of C/CZTS and C/CZTSe based systems are at −3.00 and −3.01 mA cm^{-2}, respectively. They are more negative than that of the Pt-based device (−2.50 mA cm^{-2}), indicating the reaction 1 is more efficiently preceded in the C/CZTS and C/CZTSe electrodes. Therefore, both C/CZTS and C/CZTSe on Mo/glass show stronger catalytic property for reduction reaction than that of Pt/FTO based electrode. On the other hand, the separation between the two peaks (E_{pp}) in a pair is in an inverse correlation with the standard electrochemical rate constant of the corresponding redox reaction. It is observed that the separations in the C/CZTS, C/CZTSe, and Pt electrodes are 0.650, 0.625, and 0.495 V, respectively, indicating a fast electrochemical rate in Pt/FTO based electrode. This phenomenon can be ascribed to the thickness of C/CZTS (∼730 nm) and C/CZTSe (∼450 nm) is much larger than that of Pt nanoparticles distributed on FTO surface (see Figure S1 in the Supporting Information). The ion diffusion in the C/CZTS or C/CZTSe network becomes seemingly slow. These opposite trends lead to the comparable catalytic activity in the electrodes.

In this investigation, the Mo/glass was used as a substrate to replace the FTO, which would also cause a change in series resistance because of the different conductivities. We analyzed it from the electrochemical impendence spectroscopy (EIS). The measurement was conducted on the dummy cells fabricated with two identical electrodes. Figure 3b shows the EIS results and the equivalent circuit is depicted as an inset therein. The high frequency intercept on the real axis represent the series resistance (R_s). The R_s of both C/CZTS on Mo/glass (3.4 Ω) and C/CZTSe on Mo/glass (8.3 Ω) are significantly smaller than that of the Pt/FTO based CE (23.8 Ω). This is due to the fact that the inherent conductivity of the Mo (2 Ω/□) is considerably smaller than FTO (15 Ω/□). In this case, the Mo/glass is a superior conducting substrate to FTO. It is thus easy to think that the sputtering of Pt nanoparticles on Mo glass could lead to even higher device performance. We fabricated Pt nanoparticles on the Mo/glass for the CE using the same method for sputtering Pt on FTO surface. Surprisingly, the device showed efficiency (7.90%) lower than that of Pt/FTO and C/CZTS on Mo/glass (Figure 2 and Table 1), and the performance degradation is very fast. The electrochemical characterizations are shown in Figure S6 in the Supporting Information. Only after consecutive measurement for four times does the PCE drop to 5.04%. We suspect that a Pt/Mo alloy is formed on the surface, and it is not an effective and stable catalyst for the redox reaction; further investigation is beyond the scope of current investigation. Herein, we focus on the development of a new type of Pt- and FTO-free CE.

In the EIS (Figure 3b), two maxima in the middle- and low-frequency regions stem from the charge transfer resistance (R_{ct}) and the Nernst diffusion impedance (Z) of the I_3^-/I^- couples in the electrolyte, respectively.[32] The R_{ct} of C/CZTS and C/CZTSe on Mo/glass electrodes are obtained by fitting the left arcs, which are 6.9 and 29.1 Ω, respectively, whereas that of the Pt-based electrode is 0.8 Ω. It is known that the charge transfer frequency is in an inverse correlation with the resistance. Therefore, the high frequency of charge transfer is obtained in the Pt based electrode. Similarly, this observation should be due to the thickness of the Pt nanoparticles being much smaller than those of composite catalysts. In addition, though the R_{ct} of C/CZTS is slightly higher than that of Pt/FTO, the excellent conductivity of Mo substrate is able to compensate the minor drawback,[33] finally leading to comparable catalytic properties.

To study the diffusion coefficient of the redox species, we performed Tafel polarization characterizations in dummy cells. Figure 4 shows the logarithmic current density (log J) as a function of the voltage for the oxidation/reduction reactions. The anodic and cathodic branches of C/CZTS on Mo glass display considerably larger slop than the conventional Pt and C/CZTSe electrodes, indicating a larger exchange current density (J_0) on the C/CZTS electrode surface and thus better catalytic property. On the other hand, the limiting current density, J_{lim}, is related to the diffusion coefficient in the dummy cell according to eq 3[34]

$$D = \frac{l}{2nFC} J_{lim} \quad (3)$$

dx.doi.org/10.1021/am4057375 | ACS Appl. Mater. Interfaces 2014, 6, 2224−2229

where D is the diffusion coefficient of the triiodide, l is the spacer thickness, n is the number of electrons involved in the reduction of triiodide at the electrode, F is the Faraday constant, and C is the triiodide concentration. The J_{lim} of Pt/FTO is only slightly higher than that of C/CZTS and C/CZTSe on Mo/glass (Figure 4), suggesting that network-like structures are effective for the fast diffusion of ions. Because of the good conductivity of Mo/glass and catalytic properties of the carbon supported nanodots, the final device efficiencies are superior to the Pt/FTO CE-based device.

Finally, we performed large area fabrication of the C/CZTS on Mo/glass as CE. The initial investigation is conducted by fabricating a rectangular CE with area of 100 mm × 10 mm by the "printing and annealing" method. The surface is very uniform in macroscale (Figure 5a, b), and the nanoscale structures are identical with regard to different locations (Figure 5c–e) and resemble the small-area CEs (Figure 1f). The devices fabricated using the CEs from the respective location of the large-area CE show photovoltaic parameters similar to those of the CE fabricated in small scale, confirming the scalability.

In conclusion, carbon-supported Cu_2ZnSnS_4 and $Cu_2ZnSnSe_4$ nanodots on the Mo-coated soda-lime glass have been demonstrated as efficient counter electrode materials in dye-sensitized solar cells. This type of the electrode eliminates the use of both precious Pt and high-cost FTO-based conducting substrates, and thus the materials expense of the devices can be significantly reduced. The printable procedure has been manifested to be applicable for large-area fabrication and is thus promising for industrial production. With that, the proposed method will generate broad interests in the improvement of energy conversion efficiency, reduction of the materials cost, and large-scale productions of dye-sensitized solar cells.

■ ASSOCIATED CONTENT

Supporting Information

Detail of experiment including chemicals, instrumentations, and related experimental results. This material is available free of charge via the Internet at http://pubs.acs.org.

■ AUTHOR INFORMATION

Corresponding Author

*E-mail: taochen@phy.cuhk.edu.hk.

Notes

The authors declare no competing financial interest.

■ ACKNOWLEDGMENTS

The authors acknowledge the financial support from the CUHK Group Research Scheme and CUHK Focused Scheme B Grant Center for Solar Energy Research and the University Research Grant (4053012).

■ REFERENCES

(1) Hagfeldt, A.; Boschloo, G.; Sun, L.; Kloo, L.; Pettersson, H. Dye-Sensitized Solar Cells. *Chem. Rev.* **2010**, *110*, 6595–6663.

(2) Li, L.-L.; Diau, E. W.-G. Porphyrin-Sensitized Solar Cells. *Chem. Soc. Rev.* **2013**, *42*, 291–304.

(3) Yella, A.; Lee, H. W.; Tsao, H. N.; Yi, C. Y.; Chandiran, A. K.; Nazeeruddin, M. K.; Diau, E. W. G.; Yeh, C. Y.; Zakeeruddin, S. M.; Gratzel, M. Porphyrin-Sensitized Solar Cells with Cobalt (II/III)-Based Redox Electrolyte Exceed 12 Percent Efficiency. *Science* **2011**, *334*, 629–634.

(4) Ito, S.; Murakami, T. N.; Comte, P.; Liska, P.; Grätzel, C.; Nazeeruddin, M. K.; Grätzel, M. Fabrication of thin film dye sensitized solar cells with solar to electric power conversion efficiency over 10%. *Thin Solid Films* **2008**, *516*, 4613–4619.

(5) Gao, F.; Wang, Y.; Shi, D.; Zhang, J.; Wang, M.; Jing, X.; Humphry-Baker, R.; Wang, P.; Zakeeruddin, S. M.; Grätzel, M. Enhance the Optical Absorptivity of Nanocrystalline TiO_2 Film with High Molar Extinction Coefficient Ruthenium Sensitizers for High-Performance Dye-Sensitized Solar Cells. *J. Am. Chem. Soc.* **2008**, *130*, 10720–10728.

(6) Du, Y.-F.; Fan, J.-Q.; Zhou, W.-H.; Zhou, Z.-J.; Jiao, J.; Wu, S.-X. One-Step Synthesis of Stoichiometric $Cu_2ZnSnSe_4$ as Counter Electrode for Dye-Sensitized Solar Cells. *Acs Appl. Mater. & Interfaces* **2012**, *4*, 1796–1802.

(7) Gong, F.; Wang, H.; Xu, X.; Zhou, G.; Wang, Z.-S. In Situ Growth of Co0.85Se and Ni0.85Se on Conductive Substrates as High-Performance Counter Electrodes for Dye-Sensitized Solar Cells. *J. Am. Chem. Soc.* **2012**.

(8) Wang, M.; Anghel, A. M.; Marsan, B. t.; Cevey Ha, N.-L.; Pootrakulchote, N.; Zakeeruddin, S. M.; Grätzel, M. CoS Supersedes Pt as Efficient Electrocatalyst for Triiodide Reduction in Dye-Sensitized Solar Cells. *J. Am. Chem. Soc.* **2009**, *131*, 15976–15977.

(9) Wu, M.; Lin, X.; Wang, Y.; Wang, L.; Guo, W.; Qi, D.; Peng, X.; Hagfeldt, A.; Grätzel, M.; Ma, T. Economical Pt-Free Catalysts for Counter Electrodes of Dye-Sensitized Solar Cells. *J. Am. Chem. Soc.* **2012**, *134*, 3419–3428.

(10) Roy-Mayhew, J. D.; Bozym, D. J.; Punckt, C.; Aksay, I. A. Functionalized Graphene as a Catalytic Counter Electrode in Dye-Sensitized Solar Cells. *ACS Nano* **2010**, *4*, 6203–6211.

(11) Li, G. R.; Song, J.; Pan, G. L.; Gao, X. P. Highly Pt-like Electrocatalytic Activity of Transition Metal Nitrides for Dye-Sensitized Solar Cells. *Energy Environ. Sci.* **2011**, *4*, 1680–1683.

(12) Wu, M. X.; Lin, X. A.; Hagfeldt, A.; Ma, T. L. Low-Cost Molybdenum Carbide and Tungsten Carbide Counter Electrodes for Dye-Sensitized Solar Cells. *Angew. Chem., Int. Ed.* **2011**, *50*, 3520–3524.

(13) Jiang, Q. W.; Li, G. R.; Gao, X. P. Highly ordered TiN nanotube arrays as counter electrodes for dye-sensitized solar cells. *Chem. Commun.* **2009**, 6720–6722.

(14) Lee, K. S.; Lee, H. K.; Wang, D. H.; Park, N.-G.; Lee, J. Y.; Park, O. O.; Park, J. H. Dye-Sensitized Solar Cells with Pt- and TCO-Free Counter Electrodes. *Chem. Commun.* **2010**, *46*, 4505–4507.

(15) Hou, S.; Cai, X.; Fu, Y.; Lv, Z.; Wang, D.; Wu, H.; Zhang, C.; Chu, Z.; Zou, D. Transparent Conductive Oxide-less, Flexible, and Highly Efficient Dye-Sensitized Solar Cells with Commercialized Carbon Fiber As the Counter Electrode. *J. Mater. Chem.* **2011**, *21*, 13776–13779.

(16) Zhang, T.-L.; Chen, H.-Y.; Su, C.-Y.; Kuang, D.-B. A Novel TCO- and Pt-Free Counter Electrode for High Efficiency Dye-Sensitized Solar Cells. *J. Mater. Chem. A* **2013**, *1*, 1724–1730.

(17) Hardin, B. E.; Gaynor, W.; Ding, I. K.; Rim, S.-B.; Peumans, P.; McGehee, M. D. Laminating Solution-Processed Silver Nanowire Mesh Electrodes onto Solid-State Dye-Sensitized Solar Cells. *Org. Electron.* **2011**, *12*, 875–879.

(18) Ki, W.; Hillhouse, H. W. Earth-Abundant Element Photovoltaics Directly from Soluble Precursors with High Yield Using a Non-Toxic Solvent. *Adv. Energy Mater.* **2011**, *1*, 732–735.

(19) Cheng, A.-J.; Manno, M.; Khare, A.; Leighton, C.; Campbell, S. A.; Aydil, E. S. Imaging and Phase Identification of Cu_2ZnSnS_4 Thin Films Using Confocal Raman Spectroscopy. *J. Vac. Sci. Technol. A* **2011**, *29*, -.

(20) Khare, A.; Himmetoglu, B.; Johnson, M.; Norris, D. J.; Cococcioni, M.; Aydil, E. S. Calculation of the Lattice Dynamics and Raman Spectra of Copper Zinc Tin Chalcogenides and Comparison to Experiments. *J. Appl. Phys.* **2012**, *111*, -.

(21) Wang, B.; Chang, S.; Lee, L. T. L.; Zheng, S.; Wong, K. Y.; Li, Q.; Xiao, X.; Chen, T. Improving Pore Filling of Gel Electrolyte and Charge Transport in Photoanode for High-Efficiency Quasi-Solid-

State Dye-Sensitized Solar Cells. *Acs Appl. Mater. & Interfaces* **2013**, *5*, 8289−8293.
(22) Chen, T.; Hu, W.; Song, J.; Guai, G. H.; Li, C. M. Interface Functionalization of Photoelectrodes with Graphene for High Performance Dye-Sensitized Solar Cells. *Adv. Funct. Mater.* **2012**, *22*, 5245−5250.
(23) Chang, S.; Li, Q.; Xiao, X.; Wong, K. Y.; Chen, T. Enhancement of low Energy Sunlight Harvesting in Dye-Sensitized Solar Cells Using Plasmonic Gold Nanorods. *Energy Environ. Sci.* **2012**, 9444−9448.
(24) Chen, T.; Guai, G. H.; Gong, C.; Hu, W. H.; Zhu, J. X.; Yang, H. B.; Yan, Q. Y.; Li, C. M. Thermoelectric Bi_2Te_3-Improved Charge Collection for High-Performance Dye-Sensitized Solar Cells. *Energy Environ. Sci.* **2012**, *5*, 6294−6298.
(25) Chang, S.; Wang, H.; Hua, Y.; Li, Q.; Xiao, X.; Wong, W.-K.; Wong, W. Y.; Zhu, X.; Chen, T. Conformational engineering of co-sensitizers to retard back charge transfer for high-efficiency dye-sensitized solar cells. *J. Mater. Chem. A* **2013**, *1*, 11553−11558.
(26) Joshi, P.; Xie, Y.; Ropp, M.; Galipeau, D.; Bailey, S.; Qiao, Q. Dye-sensitized Solar Cells Based on Low Cost Nanoscale Carbon/TiO_2 Composite Counter Electrode. *Energy Environ. Sci.* **2009**, *2*, 426−429.
(27) Chen, L.; Guo, C. X.; Zhang, Q.; Lei, Y.; Xie, J.; Ee, S.; Guai, G.; Song, Q.; Li, C. M. Graphene Quantum-Dot-Doped Polypyrrole Counter Electrode for High-Performance Dye-Sensitized Solar Cells. *ACS Appl. Mater. Interfaces* **2013**, *5*, 2047−2052.
(28) Wang, G.; Xing, W.; Zhuo, S. Application of Mesoporous Carbon to Counter Electrode for Dye-Sensitized Solar Cells. *J. Power Sources* **2009**, *194*, 568−573.
(29) Xue, Y.; Liu, J.; Chen, H.; Wang, R.; Li, D.; Qu, J.; Dai, L. Nitrogen-Doped Graphene Foams as Metal-Free Counter Electrodes in High-Performance Dye-Sensitized Solar Cells. *Angew. Chem., Int. Ed.* **2012**, *51*, 12124−12127.
(30) Mitzi, D. B.; Yuan, M.; Liu, W.; Kellock, A. J.; Chey, S. J.; Deline, V.; Schrott, A. G. A High-Efficiency Solution-Deposited Thin-Film Photovoltaic Device. *Adv. Mater.* **2008**, *20*, 3657−3662.
(31) Shin, B.; Gunawan, O.; Zhu, Y.; Bojarczuk, N. A.; Chey, S. J.; Guha, S. Thin Film Solar Cell with 8.4% Power Conversion Efficiency Using an Earth-Abundant Cu_2ZnSnS_4 Absorber. *Prog. Photovolt: Res. Appl.* **2013**, *21*, 72−76.
(32) Wang, Q.; Moser, J. E.; Gratzel, M. Electrochemical Impedance Spectroscopic Analysis of Dye-Sensitized Solar Cells. *J. Phys. Chem. B* **2005**, *109*, 14945−14953.
(33) Lee, B.; Buchholz, D. B.; Chang, R. P. H. An All Carbon Counter Electrode for Dye Sensitized Solar Cells. *Energy Environ. Sci.* **2012**, *5*, 6941−6952.
(34) Zhang, B.; Wang, D.; Hou, Y.; Yang, S.; Yang, X. H.; Zhong, J. H.; Liu, J.; Wang, H. F.; Hu, P.; Zhao, H. J.; Yang, H. G. *Sci. Rep.* **2013**, *3*.